

R. Lipowsky · D. Richter · K. Kremer (Eds.)

The Structure and Conformation of Amphiphilic Membranes

Proceedings
of the International Workshop
on Amphiphilic Membranes, Jülich, Germany,
September 16–18, 1991

With 150 Figures

Springer-Verlag
Berlin Heidelberg New York
London Paris Tokyo
Hong Kong Barcelona
Budapest

Contents

The Structure and Conformation of Amphiphilic Membranes: Overview By R. Lipowsky, D. Richter, and K. Kremer (With 1 Figure)	1
---	---

Part I	Molecular Structure of Membranes
---------------	---

Monolayers of Amphiphilic Molecules By H. Möhwald, R.M. Kenn, K. Kjaer, and J. Als-Nielsen (With 4 Figures)	9
The Determination of the Structure of a Mixed Surfactant Monolayer by Specular Neutron Reflection By J. Penfold, R.K. Thomas, E.M. Lee, E.A. Simister, J.R. Lu, and A.R. Rennie (With 3 Figures)	19
Does the Scanning Force Microscope Resolve Individual Lipid Molecules? By M. Radmacher, R.M. Zimmermann, and H.E. Gaub (With 5 Figures)	24
Domain Formation in a Lipid Monolayer By A. Gliozzi, A.C. Levi, M. Menessini, and E. Scalas (With 2 Figures)	30
Structure and Dynamics of Planar and Spherical Supported Phospholipid Bilayers By C. Dolainsky, T. Köchy, C. Naumann, T. Brumm, S.J. Johnson, and T.M. Bayerl (With 5 Figures)	34
Translational Diffusion and Fluid Phase Connectivity in Multi-Component, Multi-Phase Lipid Bilayer Membranes By W.L.C. Vaz, T.E. Thompson, P.F. Almeida, T. Bultmann, and E.C.C. Melo	40
Estimation of Gel and Fluid Domain Sizes in Two-Component Lipid Bilayers By M.B. Sankaram, D. Marsh, and T.E. Thompson (With 1 Figure)	45

Phosphatidyl-Glycerol in Mixtures with Positively Charged Amphiphiles: A ^2H - and ^{31}P -NMR Study of the Phase Behaviour and Headgroup Structure By R.G.K. Habiger and J. Seelig (With 3 Figures)	49
Diffusion Controlled Reactions in Two-Dimensional Space. The Pyrene Excimer Example By J.M. Martins and E.C.C. Melo (With 1 Figure)	53
Ripple Phase in Mixed Model Membrane By C. Cametti, F. De Luca, A. D'Ilario, G. Briganti, M.A. Macri, and B. Maraviglia (With 2 Figures)	57
Microscopic Theory for the Ripple Phase By R.R. Netz (With 1 Figure)	61
The Influence of Local Anaesthetics on the Temperature and Pressure Dependent Phase Behaviour of Model Biomembranes By M. Böttner, M.-H. Christmann, and R. Winter (With 7 Figures)	65
Bilayer Elasticity and Its Effects on Channel-Forming Peptides By H.W. Huang (With 5 Figures)	70
Interaction of Charged and Uncharged Calcium Channel Antagonists with Phospholipid Membranes. Binding Equilibrium, Binding Enthalpy, and Membrane Location By H.-D. Bäuerle and J. Seelig (With 2 Figures)	76
Melittin-Induced Reversible Micelle \leftrightarrow Bilayer Transition By B. Sternberg and C.E. Dempsey (With 2 Figures)	80
Theory of Hydration Forces By A.A. Kornyshev and S. Leikin	83
Force Equilibria Between Charged Surfaces with Confined Polyelectrolyte Chains By R. Podgornik (With 1 Figure)	87

Part II Conformation of Membranes

Budding Transition for Bilayer Fluid Vesicles with Area-Difference Elasticity By U. Seifert, L. Miao, H.-G. Döbereiner, and M. Wortis (With 1 Figure)	93
Some Remarks on the Shape of Toroidal Vesicles By R. Mosseri, J.F. Sadoc, and J. Charvolin (With 2 Figures)	97
The Effect of Membrane Elasticity on Shapes of Nearly Spherical Phospholipid Vesicles By F. Sevšek, S. Svetina, and B. Žekš (With 1 Figure)	101

Electron Microscopy of Biological Model Membranes By B. Klösgen and W. Helfrich (With 6 Figures)	105
Erythrocytes Membranes:	
Tethered Shells with Fluid-Like Deformation Regime By A. Zilker, H. Strey, and E. Sackmann (With 9 Figures)	113
The Isolated Human Red Blood Cell Skeleton: An Example of a Flexible Tethered Membrane	
By C.F. Schmidt, K. Svoboda, N. Lei, C.R. Safinya, S.M. Block, and D. Branton (With 3 Figures)	128
Dynamics of Flat Membranes and Flickering in Red Blood Cells By E. Frey and D.R. Nelson	133
A New Cell Model – Actin Networks Engaged by Giant Vesicles	
By M. Bärmann, J. Käs, H. Kurzmeier, and E. Sackmann (With 4 Figures)	137
Numerical Simulations of Vesicular and Red Blood Cell Shapes in Three Dimensions	
By J. Hektor, W. Form, R. Grebe, and M.J. Zuckermann (With 1 Figure)	144
Dynamic Coupling and Nonlocal Curvature Elasticity in Bilayer Membranes	
By E. Evans, A. Yeung, R. Waugh, and J. Song (With 3 Figures)	148
Phospholipid Membrane Local and Non-Local Bending Moduli Determined by Tether Formation from Aspirated Vesicles	
By S. Svetina, B. Božič, J. Song, R.E. Waugh, and B. Žekš (With 2 Figures)	154
Vesicle–Substrate Interaction Studied by Reflection Interference Contrast Microscopy	
By J. Rädler and E. Sackmann (With 5 Figures)	158
Surface Induced Fusion of Vesicles into Planar Bilayers	
By G. Cevc, W. Fenzl, and L. Sigl (With 2 Figures)	162
The Shape of an Adhered Membrane Cylinder	
By M.M. Kozlov	166
Deformation of Giant Lipid Vesicles in an Electric Field	
By M. Kummrow and W. Helfrich	170
The Effect of the Electric Field on the Shapes of Phospholipid Vesicles	
By B. Žekš and S. Svetina (With 2 Figures)	174
AC Field Controlled Formation of Giant Fluctuating Vesicles and Bending Elasticity Measurements	
By M.I. Angelova, S. Soléau, P. Méléard, J.F. Faucon, and P. Bothorel (With 3 Figures)	178

Part III Membranes in Complex Fluids

Micelles and Vesicles of Gangliosides By L. Cantù, M. Corti, and M. Musolino (With 1 Figure)	185
Self-Assembly of Bipolar Lipids By A. Relini, F. Cavagnetto, and A. Gliozzi (With 1 Figure)	189
Determination of Size and Structure of Lipid IV _A Vesicles by Quasi-Elastic Light Scattering and Small-Angle X-Ray Scattering By N. Maurer and O. Glatter (With 7 Figures)	193
Multicomponent Vesicular Aggregates (MCVA): Spontaneous Vesiculation of Perfluorinated Single-Chain Surfactant Mixtures By S. Szönyi, A. Cambon, H.J. Watzke, P. Schurtenberger, and E. Wehrli (With 3 Figures)	198
Formation of Colloid and Liquid Crystal Phases of Magnesium Dodecylbenzenesulfonate: Interpretation by Fractals By D. Težak, I. Fischer-Palković, S. Heimer, and F. Strajnar (With 3 Figures)	202
Ginzburg–Landau Theory of Bulk and Interfacial Properties of Amphiphilic Systems By G. Gompper and S. Zschocke (With 4 Figures)	206
Shape and Size Fluctuation of Microemulsion Droplets By B. Farago (With 5 Figures)	212
Microemulsions in Technical Processes By K. Stickdorn and M.J. Schwuger	218
The Effect of Additives on Surfactant Sheets in Microemulsions By M.A. Lopez-Quintela, W. Korneta, and L. Liz	222
Membrane Curvature and Structural Transitions for Charged/Uncharged Phospholipid Mixtures By D. Lerche, N.L. Fuller, and R.P. Rand (With 4 Figures)	226
Epitaxial Relationships Between Adjacent Phases in Hydrated Monoolein By R.H. Templer, N.A. Warrender, R. Meadows, and J.M. Seddon (With 2 Figures)	230
Films of Amphiphiles and Minimal Surfaces By J. Charvolin and J.F. Sadoc (With 7 Figures)	234
Phase Transitions in Cubic Amphiphilic Crystals By M. Clerc and J.F. Sadoc (With 4 Figures)	244
Elasticity and Excitations of Minimal Crystals By R. Bruinsma (With 3 Figures)	250

Inverse Micellar Cubic Phases of Lipids By J.M. Seddon and E.A. Bartle (With 1 Figure)	257
Swollen Lyotropic Cubic Phases in Fully Hydrated Mixtures of Monoolein, Dioleoylphosphatidylcholine, and Dioleoylphosphatidylethanolamine By R.H. Templer, K.H. Madan, N.A. Warrender, and J.M. Seddon (With 1 Figure)	262
Surfactant Phases with Bilayer Structures and Their Rheological Properties By C. Thunig, G. Platz, and H. Hoffmann (With 7 Figures)	266
Sponge Phases By M.E. Cates	275
Structural Inversion Processes in Three-Component Ionic Microemulsion Studied by Small Angle Neutron Scattering By S.H. Chen, S.L. Chang, R. Strey, and P. Thiyagarajan (With 3 Figures)	281
The L_3 Phase Microstructure in the AOT–Brine System has a Low Average Coordination Number By U. Olsson, B. Balinov, and O. Söderman (With 2 Figures)	287
Hydrodynamic Modes of a Viscoelastic Membrane or Interface By H. Pleiner and J.L. Harden	291
The Undulation Mode of Freely Suspended Liquid Films By H. Pleiner and H.R. Brand	295
Index of Contributors	297

Vesicle-Substrate Interaction Studied by Reflection Interference Contrast Microscopy

J. Rädler and E. Sackmann

Physik Department, Biophysics Group E22, Technische Universität München,
James Franck-Str., W-8046 Garching, Fed. Rep. of Germany

Abstract. Giant DMPC-Vesicles interacting with a supported DMPC-bilayer are investigated by Reflection Interference Contrast Microscopy (RICM). Spherical vesicles whose shape fluctuations are suppressed by osmotic pressure can be observed to fluctuate like Brownian particles above the substrate. The interaction potential can be determined from the measured distribution function of distances. In the case of adhesion, the contact contour of deflated vesicles can be calculated. Contact roundings for of weak adhesion as well as contact angles for strong adhesion have been measured.

1 Introduction

The adhesion of vesicles to a wall has recently become of interest in the context of the variety of shape transformations that free vesicles exhibit [1]. Clearly, in the case of adhering vesicles the equilibrium shape and the dynamics of the fluid membrane is strongly dependent on the strength of the vesicle wall interaction [2]. We investigated repulsive vesicle wall interaction as well as vesicle adhesion.

2 Experimental setup and methods

The experimental setup is depicted in Fig.1. The vesicles are studied by reflection interference contrast microscopy. By this technique interference is observed between the object beam reflected at the membrane and the reference beam reflected at the glass-buffer interface. In the case of an osmotically swollen, spherical vesicle the interference pattern are known as Newton rings and the absolute sphere-substrate distance can be measured from the position of the fringes. Consequently, fast image processing allows monitoring distance fluctuations in real time [3].

Furthermore, the interference fringes at the edge of the contact zone of adhering vesicles of arbitrary shape can be used to calculate the vesicle contour close to the surface. Thus the nature of the equilibrium shape of adhering vesicles in the contact zone can be studied; i.e. the contact angle for strongly adhering vesicles or smooth contact curvatures in the case of weak adhesion.

Special thought must be given to the preparation of the surface of the substrate. Since optical techniques require glass as the underlying substrate, surface

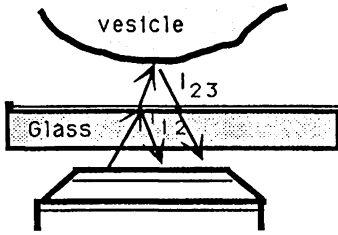


Figure 1: Principle of the reflection interference contrast microscopy. The interference between the object beam I_{23} and the reference beam I_{12} is observed.

roughness and unspecific electrostatic effects are considerable shortcomings in vesicle adhesion experiments. Most glass effects, however, are suppressed by silanizing the glass surface, i.e. chemically attaching C_{18} hydrocarbon chains to the surface and depositing a lecithin monolayer on top. Using this kind of substrate supported monolayer has the advantage of studying the symmetric lecithin-lecithin interaction that has already been measured by other techniques.

3 Repulsive interaction

Prieve et al. [4] showed recently that the interaction of a sphere which by Brownian motion fluctuates above a repulsive surface can be measured by sampling the distance distribution function of the random motion. The distribution function of distances contains the interaction potential simply by the Boltzmann relation. Giant DMPC vesicles are observed not to adhere to DMPC supported monolayers at low ionic strength ($< 20mM$) and osmotically swollen vesicles show distance fluctuations. The negative logarithm of the measured distance distribution is shown in Fig. 2. The solid line indicates a best fit to the theoretical interaction potential including electrostatic, Van der Waals and gravitational forces. The figure also shows that under the same conditions but increased ionic strength the theoretical interaction becomes attractive as experimentally observed (dashed line).

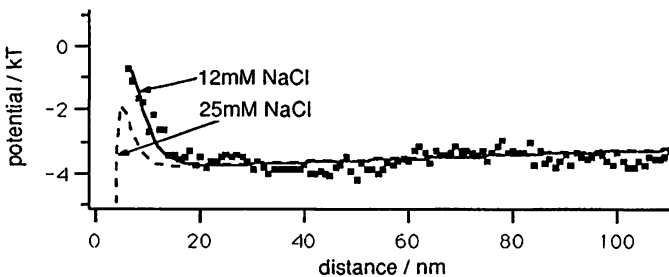


Figure 2: The interaction potential obtained from the distance fluctuations of a spherical DMPC vesicle above a DMPC supported monolayer in 100mM inositol plus 12mM NaCl. The solid line depicts the theoretical interaction potential for $\Psi = 1.8mV$. Increasing the ionic strength to 25mM leads to adhesion due to Van der Waals forces as indicated by the dashed line.

4 Weak adhesion

Adhesion is observed, if the ionic strength in a system of DMPC vesicles on a DMPC supported monolayer surface is increased to 20mM. However, the adhesion is weak which is obvious from visible surface undulations on the vesicle. Fig. 3 depicts the contour of the vesicle in the contact zone. The shape exhibits a contact rounding that is fitted by a circle of contact radius R_K (dashed line). The contact curvature has been predicted to depend on the ratio of bending to adhesion energy [6, 2] :

$$R_K = \sqrt{2K_C/\gamma} \quad (1)$$

Taking K_C to be $10^{-19} J$ the adhesion energy turns out to be on the order of $1.2 \cdot 10^{-8} J/m^2$. This value is small compared to $10^{-5} J/m^2$ measured by micropipette [6] and surface force technique [7]. However, in those cases tension is applied to the membranes, while in contrast at very low tension γ is reduced due to steric repulsion of the undulating membrane [8].

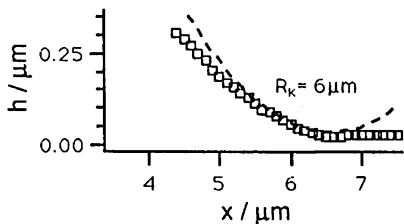


Figure 3: Calculated contour from the interference fringes of a DMPC-vesicle on a DMPC supported monolayer. The contour rounding gives an estimate for the adhesion energy. The dashed line depicts a circle of contact radius R_K (distorted scale !).

5 Strong adhesion

Strong interaction is achieved by incorporating negative charges into the supported monolayer and positive charges into the vesicle. Fig. 4 shows an example of a vesicle (SOPC:Chol:DODAB) (49:49:2 mol%) adhered to a supported monolayer (DMPC:PS) (98:2 mol%). It depicts the reconstructed profile of the vesicle. The vesicle is only slightly deflated and the contour is close to the spherical shape (dashed line). However, the contact zone exhibits sharp contact angles. The equilibrium shape of adhering vesicles has been calculated by Seifert and Lipowsky [2]. In agreement with their predictions we also found the following shapes schematically depicted in figure 5.

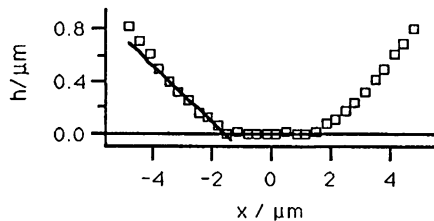


Figure 4: Reconstructed contour of a strongly adhering vesicle. The contact zone shows a contact angle.



Figure 5: Schematic representation of experimentally found shapes.

Acknowledgments

We like to thank A. Zilker for support with the image processing system. We also gratefully acknowledge the financial support by the DFG SA 246/20 and by the Fond der chemischen Industrie.

References

- [1] Kaes, J. and Sackmann, E., *Bio. Phys J.* **60** (1991) 1
- [2] Seifert, U. and Lipowsky, R., *Phys. Rev A* **42** (1990) 4768
- [3] Raedler, J. and Sackmann, E. submitted
- [4] Prieve, D.C. and Frey, N.A., *Langmuir* **6** (1990) 396
- [5] Evans, E.A. and Parsegian, V.A., in *Surface Phenomena in Hemorheology* : Copley, A.L. and Seaman, G.V.F., Eds., N.Y. Acad. Sci. (1983) 13
- [6] Evans, E.A. and Metcalf, M., *Biophys. J.* **46** (1984) 423
- [7] Marra, J. and Israelachvili, J., *Biochemistry* **24** (1985) 4608
- [8] Servuss, R.M. and Helfrich, W., *J. Phys. France* **50** (1989) 809